Transcriptome landmarks of the functional maturity of rat beta-cells, from lactation to adulthood

Carlos Larqué[1], Myrian Velasco[1], Francisco Barajas-Olmos[2], Neyvis García-Delgado[1], Juan Pablo Chávez-Maldonado[1], Jazmín García-Morales[1], Lorena Orozco[2] and Marcia Hiriart[1]

[1]Department of Neurodevelopment and Physiology, Neuroscience Division, Instituto de Fisiología Celular, Universidad Nacional Autónoma de México, Mexico City, Mexico
[2]Immunogenomics and Metabolic Disease Laboratory, Instituto Nacional de Medicina Genómica, SS, Mexico City, Mexico

Correspondence should be addressed to M Hiriart
Email
mhiriart@ifc.unam.mx

Abstract

Research on the postnatal development of pancreatic beta-cells has become an important subject in recent years. Understanding the mechanisms that govern beta-cell postnatal maturation could bring new opportunities to therapeutic approaches for diabetes. The weaning period consists of a critical postnatal window for structural and physiologic maturation of rat beta-cells. To investigate transcriptome changes involved in the maturation of beta-cells neighboring this period, we performed microarray analysis in fluorescence-activated cell-sorted (FACS) beta-cell-enriched populations. Our results showed a variety of gene sets including those involved in the integration of metabolism, modulation of electrical activity, and regulation of the cell cycle that play important roles in the maturation process. These observations were validated using reverse hemolytic plaque assay, electrophysiological recordings, and flow cytometry analysis. Moreover, we suggest some unexplored pathways such as sphingolipid metabolism, insulin-vesicle trafficking, regulation of transcription/transduction by miRNA-30, trafficking proteins, and cell cycle proteins that could play important roles in the process mentioned above for further investigation.

Introduction

Pancreatic beta-cells secrete insulin in response to changes in extracellular glucose and other secretagogues and are considered a metabolic milestone involved in regulating not only glucose but also other nutrient levels such as amino acids and lipids in the body. Postnatal development of pancreatic beta-cells has become an important subject of research in recent years not only for the achievement of the capability to differentiate progenitor or reprogramed cells into insulin-secreting cells (Mayhew & Wells 2010, Schroeder 2012, Kumar *et al*. 2014) but also to control beta-cell proliferation and maturation as a therapeutic approach in diabetes. Earlier work has suggested that cells that produce and secrete insulin can be generated using a variety of strategies (Sena *et al*. 2010, Vetere *et al*. 2014).

These insulin-secreting cells, produced *in vitro*, have characteristics similar to those of beta-cells, such as insulin-containing granules, and express beta-cell-related genes. However, these cells show a lower glucose-stimulated insulin secretion (GSIS) response or transcriptome differences compared with completely developed, normal beta-cells (D'Amour *et al.* 2006, Hrvatin *et al.* 2014, Narayanan *et al.* 2014, Pagliuca *et al.* 2014).

Previous work in our laboratory demonstrated that the rat islet development shows a critical postnatal window during the weaning period (Aguayo-Mazzucato *et al.* 2006). In accordance, it had been proposed that the mature beta-cell phenotype is determined by the capability to secrete robust amounts of insulin in basal conditions (between 4.5 and 5.6 mM glucose) and increase their insulin secretion in a correlated manner with stimulating glucose concentrations (>7 mM) (Hiriart & Aguilar-Bryan 2008). It has been suggested that the beta-cell maturation process involves changes in expression levels of ion channels related to insulin secretion (Navarro-Tableros *et al.* 2007b) and structural changes within the islet *per se*, and the islet vasculature and innervation (Cabrera-Vasquez *et al.* 2009). Furthermore, recent works had compared neonatal and adult rat beta-cell transcriptomes and observed changes in the expression levels of genes that could be involved in the maturation of the GSIS response. These genes include transcription factors such as *MafA* and *NeuroD1*; hormone receptors (Glp1r); glycolysis-, and Krebs cycle-related genes, namely *Slc2a2*, *Pfk1*, and *Pc*; metabolism/use of FAD/FMN-related genes (flavin adenine dinucleotide/flavin mononucleotide), for instance *Fmo5* and *Rfk*; and mitochondrial shuttles-related genes such as *Mdh1/2* and *Gpd1/2* (Aguayo-Mazzucato *et al.* 2011, Jermendy *et al.* 2011, Martens *et al.* 2014). However, it is possible that RNA obtained from microdissected islets could include gene transcripts from non-beta-cells, as shown by immunostaining, to determine the cell composition of rat islets at different ages (Jermendy *et al.* 2011). Moreover, it has been suggested that analyses based on differentially expressed genes may overlook effects on cellular processes or signaling pathways (Subramanian *et al.* 2005). The aim of this work was to determine the physiologic cellular context and the functional changes that could participate in the postnatal maturation process of fluorescence-activated cell sorting (FACS)-enriched populations of immature (20d) and mature (adult) rat beta-cells by the assessment of gene-set-based transcriptome analysis.

Materials and methods

Reagents

Reagents were obtained from the following sources: Hank's balanced salt solution (HBSS), ethylene glycol-bis[β-aminoethylether]*N,N,N',N'*-tetraacetic acid] (EGTA), Ficoll 400, trypan blue, poly-L-lysine, 4-(2-hydroxyethyl)-1-piperazineethanesulfonic acid (HEPES), *Staphylococcus aureus* protein A, and trypsin from Sigma-Aldrich; collagenase P from Roche; DMEM salts, penicillin–streptomycin solution, Ham F10 medium, L-glutamine solution, fetal bovine serum (FBS), and guinea pig complement from Life Technologies; bovine serum albumin lyophilized powder (BSA) from United States Biological (Swampscott, MA, USA).

Animals

The Animal Care Committee of the Instituto de Fisiología Celular, Universidad Nacional Autónoma de México approved all the methods used in this study. Animal care was performed according to the International Guiding Principles for Biomedical Research Involving Animals, Council for International Organizations of Medical Sciences, 2010.

All experiments, except microarray analysis, were carried out in neonatal (1 day postnatal), suckling (20 days old), weaning (28 days old), and young adult (250–280 g) Wistar male rats. Animals were obtained from the local animal facility and kept in a 12 h light:12 h darkness cycle. Rats were breast-fed until postnatal day 20, while weaning and young adult rats were fed with standard rat chow composed by Laboratory rodent diet 5001 (LabDiet, St. Louis, MO, USA) since postnatal day 21. Neonatal and suckling rats were fasted 4 h, and weaning and adult rats were fasted 12 h before experiments.

Islet cell culture

Before dissection, rats were anesthetized with an intraperitoneal sodium pentobarbital (40 mg/kg) injection. After surgery, animals were killed by cervical dislocation.

Pancreatic insular cells were obtained following a previously described procedure (Aguayo-Mazzucato *et al.* 2006). Briefly, pancreatic islets were obtained by collagenase digestion (0.5 mg/mL collagenase P) in Hank's balanced salt solution, Ficoll gradient centrifugation (for neonatal islets), and clean-islet handpicking (for suckling, weaning, and adult islets). Insular cells were dissociated by incubating islets in a calcium-free solution

with 5.6 mM glucose, 0.5% BSA, and 3 mM EGTA (ethylene glycol-bis(β-aminoethylether) N,N,N′,N′-tetraacetic acid) for 5 min at 37°C in a shaking bath, and 5 min more after trypsin addition (final concentration 0.01%), followed by mechanical disruption. Dissociation was stopped when 50–60% of the cells were observed as single-cell units.

Purification of single beta-cells by FACS

Before FACS, insular cells were incubated in DMEM supplemented with 0.05% BSA, 200 U/mL penicillin G, and 200 µg/mL streptomycin for 45–60 min at room temperature, and filtered through a 70 µm nylon screen to remove large clumps.

Insular cells were washed in isolation medium (123 mM NaCl, 1.8 mM $CaCl_2$, 0.8 mM $MgSO_4$, 5.4 mM KCl, 1 mM NaH_2PO_4, 2.8 mM glucose, 4.2 mM $NaHCO_3$, 10 mM HEPES, 0.5% BSA, 200 U/mL penicillin G, and 200 µg/mL streptomycin) and sorted using an FACSAria I (Beckton Dickinson) (with blue/red lasers). Purified beta-cells were received and cultured in Ham F10 medium supplemented with 10% fetal bovine serum, 200 µM L-glutamine, 200 U/penicillin G, 200 mg/mL streptomycin, and 0.5 mg/mL amphotericin.

The sorting strategy consisted in gating singlet events in the FSC-H/FSC-A plot; then, gating cells with high autofluorescence at 510–550 nm wavelength in a FITC-A/FSC-A plot; and finally, selecting cells with high SSC in an SSC-A/FITC-A plot (Fig. 1A).
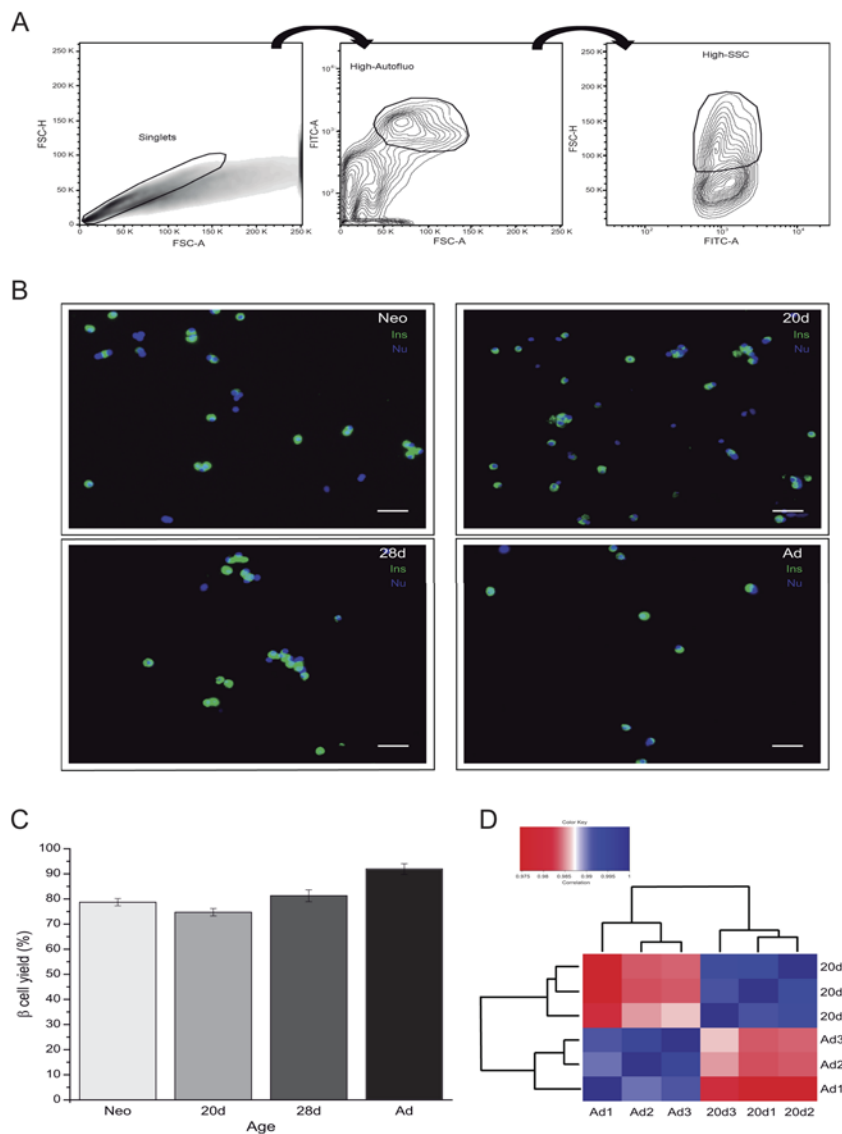

Figure 1

FACS isolation strategy and quantification of enriched beta-cell populations obtained from rats at different postnatal ages. (A) Gating strategy followed to get enriched beta-cell populations by fluorescence-activated cell sorting after primary insular cell culture from neonatal, suckling, weaning, and adult Wistar rats. (B) Insulin (green) immunostaining and nuclear counterstaining (blue) of sorted-cell populations obtained from rats of different ages. (C) Quantification of the beta-cell fraction contained in sorted populations. (D) Heat map and dendrogram that represent the global expression-level correlation among microarrays and the similarity among samples, respectively. Scale bar = 40 µm.

Published by Bioscientifica Ltd.

Immunofluorescence, purity yield and proliferation assessment

FACS-isolated beta-cells were seeded in previously poly-L-lysine-covered coverslips and cultured for 12 h at 37°C and 5% CO_2. Cells were fixed with 2% paraformaldehyde in PBS for 45 min at room temperature, rinsed with PBS, and permeabilized with a blocking-permeabilizing solution containing 2% goat serum and 0.1% Triton X (vol/vol) for 30 min at room temperature, and incubated overnight at 4°C with primary guinea pig antibody anti-insulin at 1:5000 dilution. The next day, cells were incubated for 2 h with a DyLight 483-conjugated (Jackson ImmunoResearch) or Alexa 649-conjugated (Jackson ImmunoResearch) goat anti-guinea pig IgG antibody (1:200 dilution) at room temperature, and incubated for 10 min in Hoechst 33342 (Sigma-Aldrich) solution for nuclear counterstaining. Finally, samples were mounted with medium containing 15 mM NaN_3 (DAKO). We omitted the incubation with the primary antibody for negative controls.

To analyze proliferation, primary cultured beta-cells from suckling and adult rats were seeded in poly-L-lysine-covered coverslips and cultured for 12 h at 37°C and 5% CO_2. Cells were fixed with 2% paraformaldehyde in PBS for 30 min at room temperature, rinsed with PBS, and permeabilized with a blocking-permeabilizing solution containing 10% goat serum, 0.3 M glycine, 1% bovine serum albumin, and 0.1% Tween (vol/vol) for 1 h at room temperature, and incubated overnight at 4°C with primary rabbit anti-Ki67 (ab15580) and primary guinea pig antibody anti-insulin at 1:100 and 1:5000 dilutions, respectively. The next day, cells were incubated for 1 h with an FITC (Jackson ImmunoResearch) goat anti-rabbit IgG antibody (1:100 dilution) at room temperature, rinsed with PBS, and incubated for 1 h with Alexa 649-conjugated goat anti-guinea pig IgG antibody (1:200 dilution) at room temperature. Finally, cells were incubated for 10 min in Hoechst 33342 solution for nuclear counterstaining and mounted with medium containing 15 mM NaN_3 (DAKO). Negative controls were done omitting the incubation with the primary antibodies. Positive controls were done using human cervical cancer cells (SiHa).

For imaging of specific immunoreactivity, cultured beta-cells were viewed under an epifluorescence microscope (Olympus IX7I) equipped with a 100 W mercury lamp and a filter set appropriate for Hoechst 33342 (excitation/emission wavelengths 365/440 nm), FITC (excitation/emission wavelengths 488/510 nm), and Alexa 647 (excitation/emission wavelengths 586/647 nm). Samples were observed with a 20× objective and a 1.63 zoom. Digital images were acquired with a cooled CCD digital camera (Evolution Media Cybernetics, Silver Spring, MD, USA). Exposures were chosen for the range of fluorescence intensities of each sample. Images were acquired with Image-Pro Express 2.0 software (Media Cybernetics, Silver Spring, MD, USA) and stored in TIFF image format. The beta-cell purity yield was determined by quantifying the insulin-positive cells/total cells relation, and proliferation was determined by quantifying Ki67 positive cells/insulin cells relation with ImageJ NIH, USA, software (http://rsb.info.nih.gov/ij).

RNA extraction, chip hybridization, and microarray data analysis

Total RNA was extracted using RNeasy Micro Kit (Qiagen) from three independent biological replicates per condition, each consisting of an FACS-isolated beta-cell pool obtained from four young adult or six suckling Wistar rats. Quality control was assessed by an Agilent 2100 Bioanalyzer (Agilent Technologies), taking RIN > 6.4; 200 ng total RNA were labeled and hybridized onto Affymetrix Rat GeneChip Gene 1.0 ST arrays according to manufacturer's instructions, and approximately 16,000 (according to the product data sheet) gene expression levels were obtained. Microarray data were preprocessed using R/Bioconductor software (Gentleman *et al.* 2004). Background correction, data normalization, and expression calculation were obtained by robust microarray average (RMA) method. Data have been deposited in a MIAME-compliant database (GEO series accession number GSE76969).

Expression data were assessed using gene set enrichment analysis (GSEA) to identify functionally related groups of genes (gene sets) with statistically significant enrichment at each age. Briefly, the data expression profiles from samples of both ages were ranked based on the correlation between their expression and the age distinction, and finally, determining if the members of each *a priori* defined set of genes are randomly distributed or primarily found at the top or bottom (Subramanian *et al.* 2005).

In addition, differential expression between both ages was analyzed using the R/Bioconductor package limma (Gentleman *et al.* 2004). A linear model fit was used, and differentially expressed genes were selected using a cutoff of B-statistic >0, and absolute log2 fold-change >1.5.

Reverse hemolytic plaque assay for insulin (RHPA)

Approximately, 1000 or 2000 FACS-isolated beta-cells were seeded in Cunningham chambers previously treated with

poly-L-lysine and incubated for 12 h at 37°C and 5% CO_2 in Ham F10-supplemented medium. Before the experiment, cells were incubated for 45 min at 37°C and 5% CO_2 in Hank's balanced salt solution 5.6 mM glucose; and 0.5 % BSA. A volume of 300 μL of a *Staphylococcus aureus* protein A-coated sheep erythrocytes (1:15 dilution), guinea pig insulin antiserum (1:50 dilution), and guinea pig complement (1:200 dilution) in HBSS solution with 5.6 mM glucose or 15.6 mM glucose were added to Cunningham chambers and cells were incubated for 2 h at 37°C and 5% CO_2. Insulin release was revealed by the presence of hemolytic plaques around cells, which result from the complement-mediated lysis of erythrocytes bearing insulin–anti-insulin complexes bound to protein A.

Each coverslip was scanned with a Leica Micro Dissection System 6000 (version 6.4.1.2887) coupled to a Hitachi HV-D20 camera, and the immunoplaque areas of single cells were measured using ImageJ NIH, USA, software (http://rsb.info.nih.gov/ij).

At least three independent experiments were performed by duplicate and an average of 100 cells was analyzed per experimental condition in each culture.

Cell cycle analysis by flow cytometry

Cultured insular cells were fixed with 2% paraformaldehyde in PBS for 45 min at room temperature, centrifuged and rinsed with PBS twice. After incubating with a blocking-permeabilizing solution containing 2% goat serum and 0.1% Triton X (vol/vol) for 10 min at room temperature, cells were incubated overnight at 4°C with primary guinea pig insulin antiserum at 0.8 μL/10^6 cells dilution. The next day, cells were incubated for 2 h with a DyLight 483-conjugated (Jackson ImmunoResearch) goat anti-guinea pig IgG antibody (1:200 dilution) at room temperature, and incubated for 1 h at room temperature in 1 mL DAPI (4′,6′-diamidino-2-phenylindole) solution (1 μg/mL) in order to label double-stranded DNA. The DNA content of insulin-positive single cells was acquired by an Attune Acoustic Focusing Cytometer (Life Technologies) (with blue/violet lasers), and between 10,000 and 20,000 cells were analyzed with MODFIT software (Verity Software House, Topsham, ME, USA).

Electrophysiology

Whole-cell configuration of the patch-clamp technique (Hamill *et al.* 1981) was used to record macroscopic voltage-gated Ca^{2+} currents in isolated beta-cells from suckling (20 days old) and adult rats. Recordings were done at room temperature and using an Axopatch 200A amplifier (Axon Instruments). Patch pipette was pulled from Kimax-51 capillary tube (Kimble Glass, Rockwood, TN, USA) and with resistance of 2–4 MOhms when filled with internal solution. Pipette tips were coated with dental wax to reduce pipette stray capacitance. After stable giga-seals were obtained, capacity transients of the pipette were canceled and total cell capacitance was determined by digital integration with +10 mV pulses; series resistances were compensated using the internal voltage clamp circuitry. Remaining linear capacity transients and leakage currents were subtracted by a P/2 online procedure. Pulse generation and data acquisition were performed with PClamp software version 8 (Axon Instruments).

The external solution consisted of (in mM) 130 NaCl, 5 KCl, 10 HEPES, 2 $MgCl_2$, 5 $CaCl_2$, 10 glucose, and 100 nM TTX, pH 7.3. The internal solution contained (in mM) 120 CsAsp, 10 CsCl, 5 CsF, 10 HEPES, 2.5 BAPTA, and 2 ATP, pH 7.3.

The ramp protocol used for the analysis consisted of a depolarizing pulse of 480 ms duration, from −120 to 120 mV, from a holding potential of −80 mV. Graphs show current–voltage relationship between −80 and 60 mV.

Finally, we analyzed macroscopic calcium currents of primary cultured beta-cells with capacitances between 4.5 and 11 pF ($n = 64$ for 20d cells; $n = 40$ for adult cells).

Statistical analyses

All data are reported as the mean ± S.E.M; n denotes the number of animals analyzed. The statistical significance for P value <0.01 was obtained with the one-way analysis of variance (ANOVA) and for P value <0.05 with the *t*-student test (Prism 6 for Windows Version 6.01; GraphPad Software).

Results

Morphologic and cytometric characteristics of beta-cells from different postnatal ages allow their enrichment by fluorescence-activated cell sorting

To obtain beta-cell-enriched populations, pancreatic insular cells cultured from neonatal (Neo), suckling (20d), weaning (28d), and adult (Ad) rats were submitted to FACS. After using a strategy based on the beta-cell morphologic characteristics, for instance, FSC, FAD/FADH content, and SSC for cells of all the studied ages (Fig. 1A; Materials and methods), cell sorting resulted in the recovery of beta-cell-enriched populations when assessed by immunofluorescence (near to 80 and 90% of purity when immature and mature cells were used, respectively)

(Fig. 1B and C). Interestingly, we observed that the beta-cell FAD/FADH content of neonatal, suckling, and weaning rats did not display an important difference, compared with other islet cells. However, beta-cells of adult rats showed higher FAD/FADH content than the remaining islet cells (Supplementary Fig. 1, see section on supplementary data given at the end of this article).

Beta-cell physiologic context during postnatal development depicted by transcriptome analysis using gene set enrichment analysis (GSEA)

In prior work, our research group showed that the weaning period represents a critical window for postnatal, pancreatic development (Aguayo-Mazzucato et al. 2006). We performed a microarray analysis of total RNA from immature and mature beta-cells (from 20d and adult rats) to determine the transcriptome changes involved in their maturation process. An initial assessment of the global gene expression showed a high correlation among samples from the same condition (Fig. 1D). We next performed a GSEA and a leading-edge analysis to identify (1) the functional gene sets correlated with the postnatal developmental stage of animals and (2) the core genes of those sets.

GSEA yielded a list of 155 gene sets from the Molecular Signatures Database (MSigDB), including 40 gene sets from the Reactome pathway database and 64 gene sets from the Gene Ontology (GO) collection with a positive enrichment score (Table 1), and also 1055 that include 165 gene sets from the Reactome pathway database and 163 gene sets from GO collections with a negative enrichment score (Table 2). All of them showed a false discovery rate lower than 25% and $P < 0.05$ (Supplementary Table 1).

Notably, five of the top positively enriched Reactome sets consisted of genes related to beta-cells, which include: (1) regulation of gene expression in beta-cells (NES = 2.07), (2) regulation of insulin secretion (NES = 1.94), (3) integration of energy metabolism (NES = 1.87), (4) GABA synthesis, release, reuptake, and degradation (NES = 1.85), and (5) regulation of beta-cell development (NES = 1.80) (Table 1 top).

On the other hand, the top positively enriched GO sets consisted of genes related to ion channel activity that include: (1) calcium channel activity (NES = 2.23), (2) voltage-gated calcium channel activity (NES = 2.14), (3) voltage-gated cation channel activity (NES = 2.10), and (4) voltage-gated channel activity (NES = 2.07) (Table 1 bottom). Furthermore, both the negatively enriched Reactome and GO gene sets consisted of genes related to cell proliferation (Table 2).

In addition to GSEA, we performed an analysis to obtain the genes with differential expression, and we found that 438 transcripts were upregulated in adult beta-cells and 778 were higher in 20d beta-cells (Materials and methods and Supplementary Table 2). Differential expression analysis confirmed the results observed in the studies above. Some differentially expressed genes included adult upregulated genes such as those involved in controlling beta-cell-specific gene expression and metabolism–insulin secretion coupling (Wang et al. 2007) such as MafA, Glp1r, Aplp2, Gabbr2, and 20d upregulated genes with a critical role in cell cycle regulation such as Ccna2, Ccnb1, and Ccnb2. Moreover, we found upregulation of genes that had been suggested to be involved in beta-cell maturation, which include Slc2a2 (Navarro-Tableros et al. 2007a) and Ucn3 (Blum et al. 2012, van der Meulen et al. 2012), and others such as Gcgr, Pcsk1, Igf1, Egfr, and Kcnb2.

Beta-cell transcriptome changes outline basal and GSIS maturation during postnatal development

The leading-edge analysis of the top enriched sets, namely the Reactome regulation of insulin secretion and integration of energy metabolism, showed that genes that significantly contributed to their enrichment signal also consisted of genes related to beta-cell identity and function (Fig. 2A and Table 3). To confirm the transcriptomic changes related to maturation of insulin secretion and integration of energy metabolism, basal and stimulated (glucose 5.6 and 15.6 mM) GSIS of single FACS-sorted beta-cells was assessed using RHPA (Fig. 2B). We observed that weaning and adult beta-cells secreted high basal levels of insulin. This basal secretion was represented by a 1.5-fold increase in the immunoplaque areas compared with suckling (20d) beta-cells, when exposed to basal glucose concentrations (5.6 mM) (Fig. 2B and C left panel). In addition, stimulating glucose concentrations did not produce changes on insulin secretion by neonatal beta-cells. However, suckling (20d), weaning (28d), and adult beta-cells showed a 1.3-, 1.2-, and 1.5-fold increase in insulin secretion, respectively (Fig. 2B and C right panel). Furthermore, the level of the response was correlated with the postnatal developmental stage of cells.

T-type calcium channels, among others, could participate in beta-cell maturation

It has been observed that voltage-gated calcium channels activity underlies insulin exocytosis and probably also contributes to the beta-cell maturation process

Table 1 Reactome and Gene Ontology databases gene sets correlated with the adult beta-cell phenotype (with the highest positive enrichment score).

	Name	Size	NES	NOM P value	FDR q value	FWER P value	Rank at max	Leading edge
Reactome	REGULATION OF GENE EXPRESSION IN BETA-CELLS	19	2.07	0.0	0.0036	0.004	1492	Tags = 58%, list = 11%, signal = 65%
	NEURONAL SYSTEM	257	1.97	0.0	0.011	0.025	2382	Tags = 30%, list = 17%, signal = 35%
	REGULATION OF INSULIN SECRETION	83	1.94	0.0	0.013	0.044	1128	Tags = 28%, list = 8%, signal = 30%
	TRANSMISSION ACROSS CHEMICAL SYNAPSES	175	1.88	0.0	0.026	0.111	2335	Tags = 30%, list = 17%, signal = 36%
	INTEGRATION OF ENERGY METABOLISM	106	1.87	0.0	0.024	0.126	1128	Tags = 25%, list = 8%, signal = 26%
	GABA SYNTHESIS RELEASE REUPTAKE AND DEGRADATION	17	1.85	0.005	0.028	0.1367	271	Tags = 29%, list = 2%, signal = 30%
	POTASSIUM CHANNELS	89	1.83	0.001	0.030	0.205	1947	Tags = 29%, list = 14%, signal = 34%
	INTERACTION BETWEEN L1 AND ANKYRINS	19	1.82	0.001	0.030	0.231	1961	Tags = 37%, list = 14%, signal = 43%
	RORA ACTIVATES CIRCADIAN EXPRESSION	20	1.82	0.001	0.027	0.231	3093	Tags = 75%, list = 22%, signal = 96%
	CIRCADIAN REPRESSION OF EXPRESSION BY REV ERBA	20	1.82	0.003	0.025	0.243	3093	Tags = 75%, list = 22%, signal = 96%
	GABA RECEPTOR ACTIVATION	48	1.81	0.001	0.024	0.254	2335	Tags = 38%, list = 17%, signal = 45%
	REGULATION OF BETA-CELL DEVELOPMENT	27	1.80	0.003	0.024	0.272	1875	Tags = 44%, list = 13%, signal = 51%
Gene ontology	CALCIUM CHANNEL ACTIVITY	30	2.23	0.0	0.0	0.0	1183	Tags = 40%, list = 8%, signal = 44%
	VOLTAGE-GATED CALCIUM CHANNEL ACTIVITY	17	2.14	0.0	0.004	0.001	1089	Tags = 53%, list = 8%, signal = 57%
	VOLTAGE-GATED CATION CHANNEL ACTIVITY	57	2.10	0.0	0.032	0.001	1914	Tags = 35%, list = 14%, signal = 40%
	VOLTAGE-GATED CHANNEL ACTIVITY	64	2.07	0.0	0.097	0.004	1121	Tags = 28%, list = 8%, signal = 30%
	SPHINGOLIPID METABOLIC PROCESS	27	2.04	0.0	0.001	0.009	1998	Tags = 56%, list = 14%, signal = 65%
	METAL ION TRANSMEMBRANE TRANSPORTER ACTIVITY	127	2.03	0.0	0.001	0.011	1947	Tags = 29%, list = 14%, signal = 33%
	CATION CHANNEL ACTIVITY	104	1.99	0.0	0.004	0.03	1947	Tags = 29%, list = 14%, signal = 33%
	SYNAPTIC TRANSMISSION	155	1.95	0.0	0.007	0.058	1999	Tags = 26%, list = 14%, signal = 30%
	NEURON DEVELOPMENT	55	1.94	0.0	0.007	0.066	1173	Tags = 29%, list = 8%, signal = 32%
	GATED CHANNEL ACTIVITY	108	1.91	0.0	0.011	0.109	1121	Tags = 22%, list = 8%, signal = 24%
	TRANSMISSION OF NERVE IMPULSE	168	1.89	0.0	0.014	0.147	1999	Tags = 26%, list = 15%, signal = 29%
	METAL ION TRANSPORT	100	1.89	0.0	0.014	0.163	2144	Tags = 32%, list = 15%, signal = 37%

Columns represent the name and size of the gene set; the normalized enrichment score (NES), the nominal *P* value (NOM *P* value), the false discovery rate *q* value (FDR *q* value), the family-wise error rate (FWER *P* value), the position in the ranked list at which the maximum enrichment score occurred (RANK AT MAX), and the statistics used to define the leading-edge subset (LEADING EDGE).

Table 2 Reactome and Gene Ontology databases gene sets correlated with the suckling beta-cell phenotype (with the lowest enrichment score).

	Name	Size	NES	NOM *P* value	FDR *q* value	FWER *P* value	Rank at max	Leading edge
Reactome	DNA REPLICATION	160	−3.01	0.0	0.0	0.0	1450	Tags=52%, list=10%, signal=57%
	MITOTIC M-M-G1 PHASES	140	−2.96	0.0	0.0	0.0	1450	Tags=53%, list=10%, signal=58%
	CELL CYCLE	315	−2.95	0.0	0.0	0.0	1386	Tags=42%, list=10%, signal=45%
	CELL CYCLE MITOTIC	262	−2.91	0.0	0.0	0.0	1450	Tags=42%, list=10%, signal=46%
	MITOTIC PROMETAPHASE	67	−2.76	0.0	0.0	0.0	599	Tags=48%, list=4%, signal=50%
	CELL CYCLE CHECKPOINTS	100	−2.67	0.0	0.0	0.0	2363	Tags=58%, list=17%, signal=69%
	G2-M CHECKPOINTS	39	−2.57	0.0	0.0	0.0	1201	Tags=62%, list=9%, signal=67%
	CHROMOSOME MAINTENANCE	74	−2.55	0.0	0.0	0.0	1252	Tags=49%, list=9%, signal=53%
	G1-S TRANSITION	96	−2.55	0.0	0.0	0.0	1809	Tags=52%, list=13%, signal=59%
	DEPOSITION OF NE CENPA CONTAINING NUCLEOSOMES AT THE CENTROMERE	27	−2.54	0.0	0.0	0.0	626	Tags=70%, list=4%, signal=73%
	MITOTIC G1-G1-S PHASES	114	−2.53	0.0	0.0	0.0	1914	Tags=48%, list=14%, signal=55%
	S PHASE	99	−2.50	0.0	0.0	0.0	1809	Tags=48%, list=13%, signal=55%
Gene ontology	CHROMOSOME	101	−2.64	0.0	0.0	0.0	704	Tags=31%, list=5%, signal=32%
	MITOTIC CELL CYCLE	132	−2.56	0.0	0.0	0.0	1269	Tags=33%, list=9%, signal=36%
	M PHASE OF MITOTIC CELL CYCLE	71	−2.55	0.0	0.0	0.0	1269	Tags=39%, list=9%, signal=43%
	CHROMOSOME PERICENTRIC REGION	26	−2.55	0.0	0.0	0.0	368	Tags=50%, list=3%, signal=51%
	SPINDLE	34	−2.51	0.0	0.0	0.0	368	Tags=41%, list=3%, signal=42%
	MITOSIS	68	−2.51	0.0	0.0	0.0	1269	Tags=40%, list=9%, signal=43%
	M PHASE	95	−2.49	0.0	0.0	0.0	1269	Tags=36%, list=9%, signal=38%
	CHROMOSOMAL PART	77	−2.48	0.0	0.0	0.0	704	Tags=31%, list=5%, signal=39%
	CELL CYCLE PROCESS	167	−2.47	0.0	0.0	0.0	1269	Tags=32%, list=9%, signal=34%
	CELL CYCLE PHASE	145	−2.45	0.0	0.0	0.0	1269	Tags=32%, list=9%, signal=35%
	CHROMOSOME SEGREGATION	26	−2.32	0.0	0.0	0.0	770	Tags=46%, list=5%, signal=49%
	KINETOCHORE	21	−2.27	0.0	0.0	0.0	271	Tags=43%, list=2%, signal=44%

Columns represent the name and size of the gene set; the normalized enrichment score (NES), the nominal P value (NOM p-val), the false discovery rate q value (FDR q-val), the family-wise error rate (FWER p-val), the position in the ranked list at which the maximum enrichment score occurred (RANK AT MAX), and the statistics used to define the leading-edge subset (LEADING EDGE).
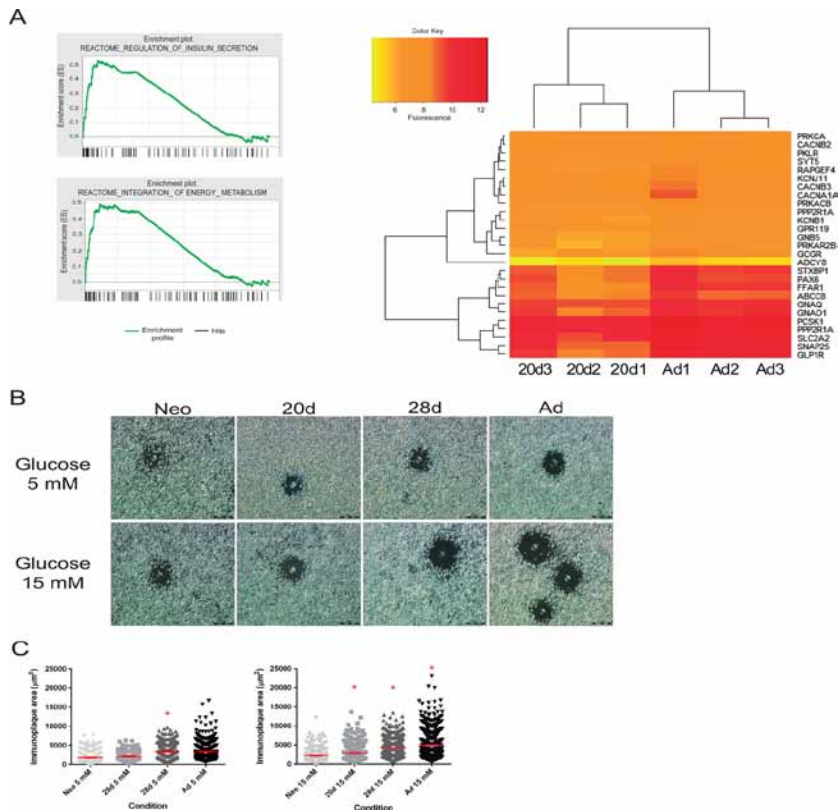
Figure 2

Basal and glucose-induced insulin secretion-related expression and physiologic changes observed in beta-cells and involved in their maturation process. (A) Enrichment plots of the Reactome regulation of insulin secretion and the Reactome integration of energy metabolism gene sets that show the running sum for each set within the beta-cell dataset (green line), and the leading-edge subset of enriched genes (vertical black lines). Heatmap of the leading-edge core genes based on their expression levels, and dendrogram depicting similarities among samples. (B) Representative images of the hemolytic immunoplaques produced by insulin secretion of neonate, suckling, weaning, and adult sorted beta-cells, incubated at basal (5.6 mM glucose; top panel) and stimulating (15.6 mM glucose; bottom panel) conditions. (C) Quantification of immunoplaque areas observed in basal (left graph) and stimulating (right graph) conditions. Red bars represent the mean + S.E.M. Scale bar = 50 μm. $^+P < 0.01$ vs the previous age, $^*P < 0.01$ vs the same age at 5.6 mM glucose.

Table 3 List of genes that contribute to the leading-edge subset within the Reactome regulation of insulin secretion gene set.

Gene symbol	Gene title	Rank in gene list	Rank metric score	Running ES
Glp1r	Glucagon-like peptide 1 receptor	22	0.54877907	0.051268473
Snap25	Synaptosomal-associated protein, 25kDa	38	0.499217749	0.09826441
Ffar1	Free fatty acid receptor 1	100	0.412623167	0.1336413
Slc2a2	Solute carrier family 2 (facilitated glucose transporter), member 2	180	0.356907934	0.16236971
Pcsk1	Proprotein convertase subtilisin/kexin type 1	199	0.346526861	0.19445017
Rapgef4	Rap guanine nucleotide exchanger factor (GEF) 4	259	0.313902557	0.22046465
Stxbp1	Syntaxin binding protein 1	271	0.307611942	0.24929762
Adcy8	Adenylate cyclase 8 (brain)	280	0.302984893	0.27789912
Cacna1a	Calcium channel, voltage-dependent, P/Q type, alpha 1 A subunit	314	0.289865345	0.30345398
Gnao1	Guanine nucleotide-binding protein (G protein), alpha activating activity polypeptide O	346	0.277311295	0.3279428
Cacnb3	Calcium channel, voltage-dependent, beta 3 subunit	387	0.263483047	0.35045815
Prkca	Protein kinase C, alpha	473	0.244811267	0.3679656
Kcnj11	Potassium inwardly rectifying cannel, subfamily J, member 11	633	0.215896025	0.37741008
Cacnb2	Calcium channel, voltage-dependent, beta 2 subunit	644	0.21452032	0.3973513
Prkacb	Protein kinase, cAMP-dependent, catalytic, beta	647	0.214400634	0.41785166
Prkar2b	Protein kinase, cAMP-dependent, regulatory, type II, beta	691	0.207862318	0.4347977
Gnb5	Guanine nucleotide binding protein (G protein), beta 5	704	0.205343723	0.4537127
Syt5	Synaptotagmin V	708	0.205186516	0.47325456
Pax6	Paired box gene 6 (aniridia, keratitis)	758	0.198414862	0.48886296
Abcc8	ATP-binding cassette, subfamily C (CFTR/MRP), member 8	873	0.185453355	0.4985865
Kcnb1	Potassium voltage-gated channel, Shab-related subfamily, member 1	1071	0.167499855	0.5006605
Gpr119	G protein-coupled receptor 119	1110	0.164306685	0.51376957
Gnaq	Guanine nucleotide-binding protein (G protein), 1 polypeptide	1128	0.163186833	0.5282689

Detailing its position, the score used to position the gene, and the enrichment score at this point in the ranked list of genes within the beta-cell dataset. Columns represent the gene symbol, the name of the gene, the position of the gene in the ranked list of genes, the score used to position the gene in the ranked list, and the enrichment score at this point in the ranked list of genes.

Table 4 List of genes that contribute to the leading-edge subset within the GO calcium channel activity gene set.

Gene symbol	Gene title	Rank in gene list	Rank metric score	Running ES
Trpc5	Transient receptor potential cation channel, subfamily C, member 5	42	0.489	0.1158
Cacna2d1	Calcium channel, voltage-dependent, alpha 2/delta subunit 1	55	0.472	0.2295
Cacna1c	Calcium channel, voltage-dependent, L type, alpha 1 C subunit	206	0.343	0.3021
Cacna1b	Calcium channel, voltage-dependent, L type, alpha 1B subunit	260	0.313	0.3743
Cacna1h	Calcium channel, voltage-dependent, alpha 1H subunit	294	0.297	0.4442
Cacna1a	Calcium channel, voltage-dependent, P/Q type, alpha 1ª subunit	314	0.290	0.5132
Cacnb3	Calcium channel, voltage-dependent, beta 3 subunit	387	0.263	0.5720
Cacnb2	Calcium channel, voltage-dependent, beta 2 subunit	644	0.215	0.6059
Trpc1	Transient receptor potential cation channel, subfamily C, member 1	716	0.204	0.6504
Cacna1d	Calcium channel, voltage-dependent, L type, alpha 1 D subunit	799	0.194	0.6915
Cacnb1	Calcium channel, voltage-dependent, beta 1 subunit	1089	0.166	0.7114
Ms4a2	Membrane-spanning 4-domains, subfamily A, member 2 (Fc fragment of IgE, high affinity I, receptor for; beta polypeptide)	1183	0.158	0.7433

We detailed its place, the score used to position the gene, and the enrichment score at this point in the ranked list of genes within the beta-cell dataset. Columns represent the gene symbol, the name of the gene, the position of the gene in the ranked list of genes, the score used to position the gene in the ranked list, and the enrichment score at this point in the ranked list of genes.

(Navarro-Tableros *et al.* 2007*b*). We considered the top enriched GO gene sets (Table 4) further to investigate the phenotype correlation of the *Cacna1h* gene with maturation (Fig. 3A). We performed whole-cell recordings of macroscopic calcium currents from cultured, immature (20d), and mature (adult) beta-cells. Both immature and mature cells showed T-type calcium currents, within the expected membrane potential interval, from −40 to −10 mV (Fig. 3B) (Materials and methods). Furthermore, we observed that 85% of adult beta-cells showed T-type calcium currents compared with 59% of 20d beta-cells (Fig. 3C).

Acquisition of a mature beta-cell phenotype involves the loss of replicative capabilities

As shown in Table 2, the Reactome and GO databases' bottom-enriched sets are related to cell proliferation. Thus, we first assessed beta-cell proliferation from suckling rats by Ki67 immunofluorescence and observed a low proliferation rate (data not shown). However, the leading-edge analysis results consisted of genes related to cell cycle progressions such as *E2F1, Tp53, Ccna2*, and *Ccnb1* (Fig. 4A top panel and Table 5). Moreover, some of these core genes showed changes in their expression levels (Fig. 4A lower panel). Accordingly, with these results, we investigated the distribution of the cell cycle phases within suckling, weaning, and adult beta-cells by flow cytometry (Fig. 4B). We observed, on one hand, that the proportion of adult beta-cells at G1 cell cycle phase (87.9%) was higher compared with suckling (20d) and weaning (28d) beta-cells (79.1% for both). On the other

hand, the percentage of weaning (28d) and adult beta-cells at S phase (2.12 and 0.65%, respectively), and that of adult cells at G2/M phase (11.4%), decreased when compared with suckling (20d) beta-cells (16.1% for G2/M, and 4.6% for S phase of the cell cycle) (Fig. 4C, see asterisks at insets, and Fig. 4D).

Discussion

Postnatal maturation of pancreatic beta-cells is an important research area due to the increasing interest in the *in vitro* generation of insulin-secreting cells to treat both type 1 and type 2 diabetes mellitus. Previous works had shown that a physiological critical window that consists of the suckling and weaning periods plays a significant role in rat beta-cell development and lifespan function (Aguayo-Mazzucato *et al.* 2006, Cabrera-Vasquez *et al.* 2009, Stolovich-Rain *et al.* 2015). Research on the development, including the postnatal period, of pancreatic beta-cells could generate significant knowledge to, on one hand, improve the generation of mature insulin-producing cells as a source for diabetes cell-based therapies and, on the other hand, to stimulate *in situ* beta-cell division to overcome insulin deficiency observed during diabetes.

Fluorescence-activated cell sorting is a useful tool to study a wide variety of biological processes in a particular type of cell. In previous work, different research groups used this approach to study beta-cells obtained from adult rats (Pipeleers *et al.* 1985, Kohler *et al.* 2012) and, recently, from neonatal rats (Martens *et al.* 2014).
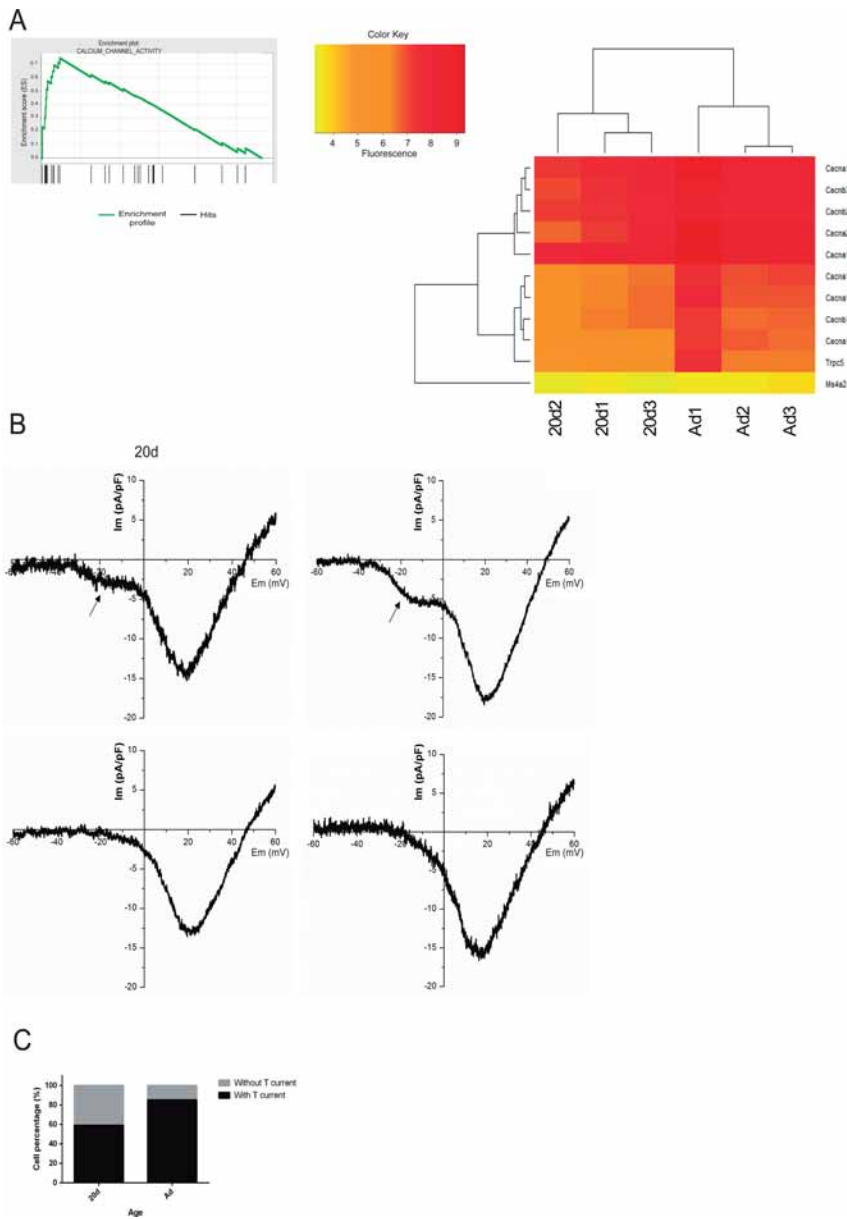
Figure 3
Calcium channels expression and functional changes that contribute, in part, to the maturation of basal and glucose-induced insulin secretion observed in beta-cells. (A) Enrichment plot of the GO calcium channel activity gene set that show the running sum for the set within the beta-cell dataset (green line), and the leading-edge subset of enriched genes (vertical black lines). Heat map of the leading-edge core genes based on their expression levels and a dendrogram is depicting similarities among samples. (B) Representative recordings of global calcium channel currents observed in 20d and adult beta-cells. Arrows represent T-type calcium channel current. (C) Quantification of the beta-cell percentage with and without T-type calcium channel current (gray: percentage of cells without T-type calcium current; black: percentage of cells with T-type calcium current). A full colour version of this figure is available at http://dx.doi.org/10.1530/JME-16-0052.

In the present work, we purified and cultured pancreatic beta-cells from rats between postnatal day 1 and 10 weeks old, isolated by flow cytometry. We observed that the more mature the cells were, the higher the beta-cell purity yield we obtained. This fact could be related to the gradual acquisition of certain morphologic characteristics such as size (FSC), internal complexity (SSC), and autofluorescence (FITC) during early postnatal development, which could probably identify a beta-cell among others within the mature pancreatic islet (Supplementary Fig. 1). For instance, we consider that FACS consists of a valuable tool for culturing enriched beta-cell populations compared with those obtained from primary cultures.

Gene-set, enrichment-based transcriptome analysis provides a large list of curated gene sets that not only shows the top-ranked signaling pathways, functions, or processes that are enriched in a correlated manner with a specific cell phenotype but also allows a comparison with those whose changes during development could contribute the most to the phenotype acquisition. First, we performed a GSEA to outline the gene sets that characterize mature beta-cell physiology. Interestingly, we obtained a list of 155 gene sets that include some that could be expected beta-cell maturity-related sets, such as regulation of gene expression in beta-cells, regulation of beta-cell development, and insulin secretion. Also, we obtained
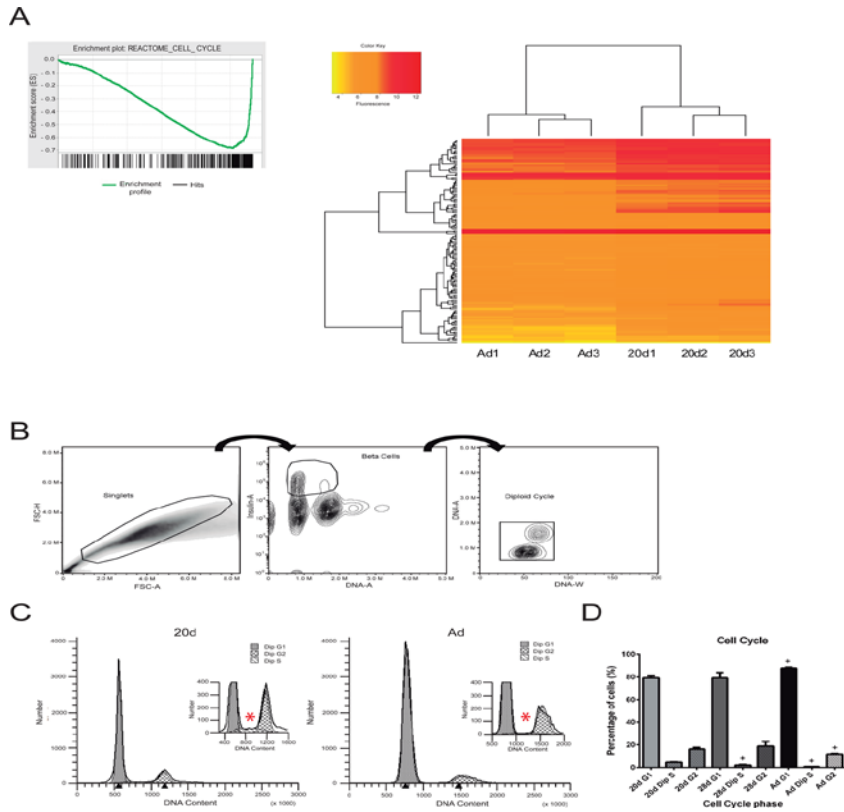
Figure 4

Cell-cycle-related expression and functional changes observed in beta-cells and involved in the transition from a proliferating phenotype to a quiescent one. (A) Enrichment plots of the Reactome cell cycle gene set that show the running sum for the set within the beta-cell dataset (green line), and the leading-edge subset of enriched genes (vertical black lines). Heatmap of the leading-edge core genes based on their expression levels and a dendrogram is depicting similarities among samples. (B) The gating strategy followed to assess beta-cell cycle after primary insular cell culture from Wistar rats at different ages. (C) Representative histograms of DNA content from beta-cells of suckling and adult rats. (Insets) Histogram zoom to show the S and G2/M phases. (D) Quantification of the percentage of beta-cells from different ages at each cell-cycle phase. $^{+}P < 0.05$ vs the same cell cycle phase at 20d. A full colour version of this figure is available at http://dx.doi.org/10.1530/JME-16-0052.

Table 5 List of genes that contribute to the leading-edge subset within the Reactome cell cycle gene set.

Gene symbol	Gene title	Rank in gene list	Rank metric score	Running ES
Bub1b	BUB1 budding uninhibited by benzimidazoles 1 homolog beta (yeast)	13,991	−0.503589034	−0.2868474
Mybl2	V-myb myeloblastosis viral oncogene homolog (avian)-like 2	13,999	−0.523670435	−0.27833852
Dsn1	DSN1, MIND kinetochore complex component, homolog (*S. cerevisiae*)	14,008	−0.549398065	−0.26945922
Kif2c	Kinesin family member 2C	14,010	−0.563030958	−0.2598374
Kif18a	Kinesin family member 18A	14,017	−0.576656222	−0.25034368
Cdc20	CDC20 cell division cycle 20 homolog (*S. cerevisiae*)	14,018	−0.580106974	−0.2403553
Mad2l1	MAD2 mitotic arrest deficient-like 1 (yeast)	14,019	−0.580602169	−0.2303584
Ccnb2	Cyclin B2	14,020	−0.581152618	−0.22035204
Gins1	GINS complex subunit 1 (Psf1 homolog)	14,023	−0.603614151	−0.21010399
Pttg1	Pituitary tumor-transforming 1	14,028	−0.619677007	−0.19972445
Plk1	Polo-like kinase 1 (Drosophila)	14,036	−0.640498042	−0.189204
Hist1h2bb	Histone cluster 1, H2bb	14,037	−0.644302547	−0.17811032
Mlf1ip	MLF1-interacting protein	14,039	−0.64978236	−0.1669948
Cenpi	Centromere protein I	14,047	−0.678234518	−0.15582462
Ccnb1	Cyclin B1	14,056	−0.691223979	−0.14450333
Nuf2	NUF2, NDC80 kinetochore complex component, homolog (*S. cerevisiae*)	14,062	−0.717477024	−0.13251238
Ska1	Spindle and kinetochore associated complex subunit 1	14,065	−0.734317064	−0.12001387
Spc25	SPC25, NDC80 kinetochore complex component, homolog (*S. cerevisiae*)	14,074	−0.804355443	−0.13674466
Ccna2	Cyclin A2	14,078	−0.842607439	−0.09245413
Sgol2	Shugoshin-like 2 (*S. pombe*)	14,080	−0.846453488	−0.0779523
Ndc80	NDC80 homolog, kinetochore complex component (*S. cerevisiae*)	14,083	−0.873560488	−0.06305628
Rrm2	Ribonucleotide reductase M2 polypeptide	14,085	−0.922827721	−0.048064876
Cenpk	Centromere protein K	14,090		−0.03246564
Cdk1	Cyclin-dependent kinase 1	14,092	−0.932636738	−0.016479896
Bub1	BUB1 budding uninhibited by benzimidazoles 1 homolog (yeast)	14,094	−0.986617088	4.35E-04

Detailing its place, the score used to position the gene, and the enrichment score at this point in the ranked list of genes within the beta-cell dataset. Columns represent the gene symbol, the name of the gene, the position of the gene in the ranked list of genes, the score used to position the gene in the ranked list, and the enrichment score at this point in the ranked list of genes.

new beta-cell maturity-related gene sets, such as potassium channel activity, sphingolipid metabolism, transmission across chemical synapses, and miRNA-30 target genes (Supplementary Tables 1, 3, and 4).

Our validation approach confirmed that mature beta-cells contain fully developed secretory machinery and integrate metabolic inputs in a more efficient manner. Recent work had shown that sphingosine kinase 2 (*Sphk2*) activation and a rise in S1P levels due to glucose stimulation play an important role in GSIS. Thus, further research on this new beta-cell maturity-related gene set would be needed to assess their role in the beta-cell maturation process (Cantrell Stanford *et al.* 2012). Moreover, a different research group had suggested that miR-30 family microRNAs maintain the epithelial phenotype of pancreatic islet cells (Joglekar *et al.* 2009) though it would also be interesting to assess their role in the beta-cell postnatal development and the GSIS. Finally, it has been demonstrated that the molecular machinery of insulin exocytosis in beta-cells consists of a variety of proteins very similar to that observed in synaptic vesicle release (Hou *et al.* 2009). However, the physiologic role of these proteins during beta-cell maturation remains unknown, and further work is needed.

GSEA also yielded a large list of gene sets whose decreased activity could be associated with the loss of a replicating and immature phenotype. We decided to validate these observations using flow cytometry analysis to determine the distribution of the cycle phases within beta-cell populations obtained from suckling, weaning, and adult rats.

A recent work analyzed the cell cycle progression using the Fucci system in transformed fetal human pancreatic beta-cell lines. Their results showed that the induction of advanced differentiation is correlated with the exit from the cell cycle of these cells (Carlier *et al.* 2014). Our results showed that immature beta-cells actively transcribe proliferation-related genes and that a higher percentage of beta-cells from suckling and weaning rats could be found at S and G2/M phases of the cell cycle when compared with beta-cells from adult rats. However, the majority of beta-cells at all ages were found at the G1/G0 phase. Although postnatal beta-cell replication and apoptosis have been described before (Scaglia *et al.* 1997, Kulkarni *et al.* 2012), to our knowledge, this is the first work that analyzes primary cultured rat beta-cell progression among the cell cycle phases during rat postnatal maturation.

Moreover, Annicote and coworkers observed that some canonical cell-cycle-related gene products such as CDK4, pRB, and E2F1 could be involved in the transcriptional regulation of insulin secretion-related genes such as *Kcnj11* (Kir6.2, which is a component of the KATP channel). Also, they demonstrated that the CDK4-pRB-E2F1 pathway could be regulated by insulin signaling in mouse pancreatic islets (Annicotte *et al.* 2009). This observation could explain in part why beta-cells from suckling rats show low proliferation rates (tested by Ki67 immunofluorescence, data not shown) despite their high expression of cell-cycle-related genes, indicating that the beta-cells' proliferative capability is inversely correlated with the basal robust insulin secretion and the glucose-stimulated insulin secretion functions.

To our knowledge, our lab was the first to propose the weaning period as a critical maturation window of pancreatic development, and suggest that dietary changes in carbohydrates and lipids composition play a highlighting role in GSIS maturation (Aguayo-Mazzucato *et al.* 2006). Furthermore, recent work has observed that mice prematurely weaned to a high-fat diet resembling milk showed a lower increase in plasma insulin in response to glucose compared with mice prematurely weaned to a normal chow diet (Stolovich-Rain *et al.* 2015). These data point to the leading role of diet over age in the maturation of the beta-cell GSIS.

This work highlights the relevance of the molecular machinery of insulin exocytosis and the cell cycle pathway roles in the maturation process of pancreatic beta-cells. Moreover, future work to elucidate pathways that could control either the role of these exocytic proteins or the cell cycle proteins will bring new opportunities to expand beta-cell populations to treat diabetes.

Declaration of interest
The authors declare that there is no conflict of interest that could be perceived as prejudicing the impartiality of the research reported.

References

Aguayo-Mazzucato C, Sanchez-Soto C, Godinez-Puig V, Gutierrez-Ospina G & Hiriart M 2006 Restructuring of pancreatic islets and insulin secretion in a postnatal critical window. *PLoS ONE* **1** e35. (doi:10.1371/journal.pone.0000035)

Aguayo-Mazzucato C, Koh A, El Khattabi I, Li WC, Toschi E, Jermendy A, Juhl K, Mao K, Weir GC, Sharma A, *et al.* 2011 Mafa expression enhances glucose-responsive insulin secretion in neonatal rat beta cells. *Diabetologia* **54** 583–593. (doi:10.1007/s00125-010-2026-z)

Annicotte JS, Blanchet E, Chavey C, Iankova I, Costes S, Assou S, Teyssier J, Dalle S, Sardet C & Fajas L 2009 The CDK4-pRB-E2F1 pathway controls insulin secretion. *Nature Cell Biology* **11** 1017–1023. (doi:10.1038/ncb1915)

Blum B, Hrvatin SS, Schuetz C, Bonal C, Rezania A & Melton DA 2012 Functional beta-cell maturation is marked by an increased glucose threshold and by expression of urocortin 3. *Nature Biotechnology* **30** 261–264. (doi:10.1038/nbt.2141)

Cabrera-Vasquez S, Navarro-Tableros V, Sanchez-Soto C, Gutierrez-Ospina G & Hiriart M 2009 Remodelling sympathetic innervation in rat pancreatic islets ontogeny. *BMC Developmental Biology* **9** 34. (doi:10.1186/1471-213X-9-34)

Cantrell Stanford J, Morris AJ, Sunkara M, Popa GJ, Larson KL & Ozcan S 2012 Sphingosine 1-phosphate (S1P) regulates glucose-stimulated insulin secretion in pancreatic beta cells. *Journal of Biological Chemistry* **287** 13457–13464. (doi:10.1074/jbc.M111.268185)

Carlier G, Maugein A, Cordier C, Pechberty S, Garfa-Traore M, Martin P, Scharfmann R & Albagli O 2014 Human fucci pancreatic Beta cell lines: new tools to study Beta cell cycle and terminal differentiation. *PLoS ONE* **9** e108202. (doi:10.1371/journal.pone.0108202)

D'Amour KA, Bang AG, Eliazer S, Kelly OG, Agulnick AD, Smart NG, Moorman MA, Kroon E, Carpenter MK & Baetge EE 2006 Production of pancreatic hormone-expressing endocrine cells from human embryonic stem cells. *Nature Biotechnology* **24** 1392–1401. (doi:10.1038/nbt1259)

Gentleman RC, Carey VJ, Bates DM, Bolstad B, Dettling M, Dudoit S, Ellis B, Gautier L, Ge Y, Gentry J, *et al.* 2004 Bioconductor: open software development for computational biology and bioinformatics. *Genome Biology* **5** R80. (doi:10.1186/gb-2004-5-10-r80)

Hamill OP, Marty A, Neher E, Sakmann B & Sigworth FJ 1981 Improved patch-clamp techniques for high-resolution current recording from cells and cell-free membrane patches. *Pflügers Archiv* **391** 85–100. (doi:10.1007/BF00656997)

Hiriart M & Aguilar-Bryan L 2008 Channel regulation of glucose sensing in the pancreatic beta-cell. *American Journal of Physiology: Endocrinology and Metabolism* **295** E1298–E1306. (doi:10.1152/ajpendo.90493.2008)

Hou JC, Min L & Pessin JE 2009 Insulin granule biogenesis, trafficking and exocytosis. *Vitamins & Hormones* **80** 473–506. (doi:10.1016/S0083-6729(08)00616-X)

Hrvatin S, O'Donnell CW, Deng F, Millman JR, Pagliuca FW, DiIorio P, Rezania A, Gifford DK & Melton DA 2014 Differentiated human stem cells resemble fetal, not adult, beta cells. *PNAS* **111** 3038–3043. (doi:10.1073/pnas.1400709111)

Jermendy A, Toschi E, Aye T, Koh A, Aguayo-Mazzucato C, Sharma A, Weir GC, Sgroi D & Bonner-Weir S 2011 Rat neonatal beta cells lack the specialised metabolic phenotype of mature beta cells. *Diabetologia* **54** 594–604. (doi:10.1007/s00125-010-2036-x)

Joglekar MV, Patil D, Joglekar VM, Rao GV, Reddy DN, Mitnala S, Shouche Y & Hardikar AA 2009 The miR-30 family microRNAs confer epithelial phenotype to human pancreatic cells. *Islets* **1** 137–147. (doi:10.4161/isl.1.2.9578)

Kohler M, Dare E, Ali MY, Rajasekaran SS, Moede T, Leibiger B, Leibiger IB, Tibell A, Juntti-Berggren L & Berggren PO 2012 One-step purification of functional human and rat pancreatic alpha cells. *Integrative Biology* **4** 209–219. (doi:10.1039/c2ib00125j)

Kulkarni RN, Mizrachi EB, Ocana AG & Stewart AF 2012 Human beta-cell proliferation and intracellular signaling: driving in the dark without a road map. *Diabetes* **61** 2205–2213. (doi:10.2337/db12-0018)

Kumar SS, Alarfaj AA, Munusamy MA, Singh AJ, Peng IC, Priya SP, Hamat RA & Higuchi A 2014 Recent developments in beta-cell differentiation of pluripotent stem cells induced by small and large molecules. *International Journal of Molecular Sciences* **15** 23418–23447. (doi:10.3390/ijms151223418)

Martens GA, Motte E, Kramer G, Stange G, Gaarn LW, Hellemans K, Nielsen JH, Aerts JM, Ling Z & Pipeleers D 2014 Functional characteristics of neonatal rat beta cells with distinct markers. *Journal of Molecular Endocrinology* **52** 11–28. (doi:10.1530/JME-13-0106)

Mayhew CN & Wells JM 2010 Converting human pluripotent stem cells into beta-cells: recent advances and future challenges. *Current Opinion in Organ Transplantation* **15** 54–60. (doi:10.1097/MOT.0b013e3283337e1c)

Narayanan K, Lim VY, Shen J, Tan ZW, Rajendran D, Luo SC, Gao S, Wan AC & Ying JY 2014 Extracellular matrix-mediated differentiation of human embryonic stem cells: differentiation to insulin-secreting beta cells. *Tissue Engineering Part A* **20** 424–433. (doi:10.1089/ten.tea.2013.0257)

Navarro-Tableros V, Fiordelisio T, Hernandez-Cruz A & Hiriart M 2007*a* Nerve growth factor promotes development of glucose-induced insulin secretion in rat neonate pancreatic beta cells by modulating calcium channels. *Channels* **1** 408–416. (doi:10.4161/chan.1.6.5450)

Navarro-Tableros V, Fiordelisio T, Hernandez-Cruz A & Hiriart M 2007*b* Physiological development of insulin secretion, calcium channels, and GLUT2 expression of pancreatic rat beta-cells. *American Journal of Physiology: Endocrinology and Metabolism* **292** E1018–E1029. (doi:10.1152/ajpendo.00457.2006)

Pagliuca FW, Millman JR, Gurtler M, Segel M, Van Dervort A, Ryu JH, Peterson QP, Greiner D & Melton DA 2014 Generation of functional human pancreatic beta cells in vitro. *Cell* **159** 428–439. (doi:10.1016/j.cell.2014.09.040)

Pipeleers DG, in't Veld PA, Van de Winkel M, Maes E, Schuit FC & Gepts W 1985 A new in vitro model for the study of pancreatic A and B cells. *Endocrinology* **117** 806–816. (doi:10.1210/endo-117-3-806)

Scaglia L, Cahill CJ, Finegood DT & Bonner-Weir S 1997 Apoptosis participates in the remodeling of the endocrine pancreas in the neonatal rat. *Endocrinology* **138** 1736–1741. (doi:10.1210/endo.138.4.5069)

Schroeder IS 2012 Potential of pluripotent stem cells for diabetes therapy. *Current Diabetes Reports* **12** 490–498. (doi:10.1007/s11892-012-0292-5)

Journal of Molecular Endocrinology

Sena CM, Bento CF, Pereira P & Seica R 2010 Diabetes mellitus: new challenges and innovative therapies. *EPMA Journal* **1** 138–163. (doi:10.1007/s13167-010-0010-9)

Stolovich-Rain M, Enk J, Vikesa J, Nielsen FC, Saada A, Glaser B & Dor Y 2015 Weaning triggers a maturation step of pancreatic beta cells. *Developmental Cell* **32** 535–545. (doi:10.1016/j.devcel.2015.01.002)

Subramanian A, Tamayo P, Mootha VK, Mukherjee S, Ebert BL, Gillette MA, Paulovich A, Pomeroy SL, Golub TR, Lander ES, *et al*. 2005 Gene set enrichment analysis: a knowledge-based approach for interpreting genome-wide expression profiles. *PNAS* **102** 15545–15550. (doi:10.1073/pnas.0506580102)

van der Meulen T, Xie R, Kelly OG, Vale WW, Sander M & Huising MO 2012 Urocortin 3 marks mature human primary and embryonic stem cell-derived pancreatic alpha and beta cells. *PLoS ONE* **7** e52181. (doi:10.1371/journal.pone.0052181)

Vetere A, Choudhary A, Burns SM & Wagner BK 2014 Targeting the pancreatic beta-cell to treat diabetes. *Nature Reviews Drug Discovery* **13** 278–289. (doi:10.1038/nrd4231)

Wang H, Brun T, Kataoka K, Sharma AJ & Wollheim CB 2007 MAFA controls genes implicated in insulin biosynthesis and secretion. *Diabetologia* **50** 348–358. (doi:10.1007/s00125-006-0490-2)